ACS APPLIED MATERIALS & INTERFACES

Research Article

www.acsami.org

Hierarchical Macroporous Zn_2SnO_4–ZnO Nanorod Composite Photoelectrodes for Efficient CdS/CdSe Quantum Dot Co-Sensitized Solar Cells

Long-Bin Li, Yu-Fen Wang, Hua-Shang Rao, Wu-Qiang Wu, Ke-Nan Li, Cheng-Yong Su, and Dai-Bin Kuang*

MOE Key Laboratory of Bioinorganic and Synthetic Chemistry, KLGHEI of Environment and Energy Chemistry, State Key Laboratory of Optoelectronic Materials and Technologies, School of Chemistry and Chemical Engineering, Sun Yat-sen University, Guangzhou 510275, P. R. China

ABSTRACT: A hierarchical macroporous Zn_2SnO_4–ZnO nanorod composite film is prepared through a drop-casting process of PS@Zn_2SnO_4 and subsequent hydrothermal growth of ZnO nanorod. CdS/CdSe co-sensitized solar cells based on the macroporous Zn_2SnO_4–ZnO nanorod composite photoelectrode exhibits an enhancement of 34.4% in power conversion efficiency (1.68%) compared to the pristine macroporous Zn_2SnO_4 photoelectrode (1.25%). Especially worth noting is that the growth of ZnO nanorods contributes greatly to the enlargement of surface area and improvement of light scattering ability of the composite film, which dominates the increase of J_{sc} values and eventual power conversion efficiency. QDSSCs based on the optimized 9 μm thick composite photoanode film exhibits a power conversion efficiency of 2.08%, which is the highest value for the reported QDs sensitized solar cells based on the Zn_2SnO_4 photoelectrode.

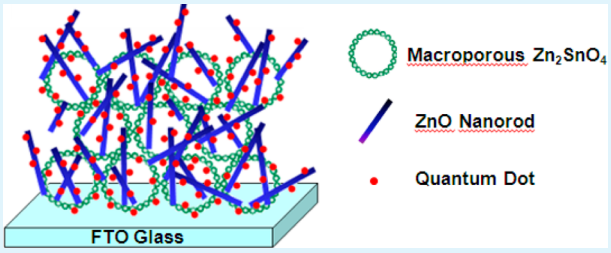

KEYWORDS: *macroporous Zn_2SnO_4, ZnO nanorods, electrodeposition, CdS, CdSe, quantum dot-sensitized solar cells*

INTRODUCTION

Quantum dot-sensitized solar cell (QDSSC), as the third generation solar cell, has drawn intense attention recently due to its low cost as well as impressive power conversion efficiency. The morphology, size, and structure of photoanode materials were found to play vital roles in the sensitizer loading amount, electron transport, and recombination as well as light scattering, which would influence the overall photovoltaic performance of QDSSCs.[1−11] Up until now, TiO_2 and ZnO were the most commonly used materials as photoanodes for QDSSCs. On top of that, some other inorganic semiconductors have also been introduced as photoanode materials in the recent past few years. Especially worth noting is Zn_2SnO_4, a ternary oxide semiconductor, which has been reported to possess a wide band gap of 3.6 eV and large electron mobility of 10−15 $cm^2\ V^{-1}\ s^{-1}$,[12] which is superior to that of TiO_2 (0.1−1.0 $cm^2\ V^{-1}\ s^{-1}$).[13] The earliest research based on Zn_2SnO_4 photoanodes for dye-sensitized solar cells (DSSCs) stemmed from 2007,[14,15] and showed an energy conversion efficiency of 3.8%.[15] Subsequently, the investigations based on different morphologies of Zn_2SnO_4 such as nanoparticles, nanowires, or octahedra have been reported.[16−22] Recently, the macroporous or hollow Zn_2SnO_4 based photoelectrode showed an impressive high efficiency of 6.10% when applied in DSSCs.[23] From another perspective, Zn_2SnO_4 showcased its possibility to be a potential candidate for QDSSCs.[24−27] For instance, Dai et al. loaded CdSe QDs on Zn_2SnO_4 nanowires with the pulsed laser deposition method, and the as-prepared QDSSC exhibited a conversion efficiency of 0.3%.[26] Bora et al. covered ZnO nanorods with Zn_2SnO_4 nanoparticles to fabricate a composite photoanode for CdS QDSSCs which showed the highest efficiency (1.24%) for Zn_2SnO_4 photoelectrode based QDSSC up to now.[27]

Hierarchical assembly of hybrid nanostructure with nanoscale building blocks has attracted immense interests for solar cell application. In some cases, some kinds of composite photoelectrodes such as TiO_2–ZnO,[28−31] SnO_2–TiO_2,[32] ZnO-Zn_2SnO_4,[27] and SnO_2–Zn_2SnO_4[33] exhibited superior photovoltaic performance in QDSSCs or DSSCs. It is generally believed that hollow materials possess fast electron transport paths (from ordered networks), enhanced light scattering (from ordered macropores), and fast mass transport especially for the quasi- or all solid state electrolyte with a high viscosity and thus being intensively investigated as photoelectrode.[34−37] Recently, hierarchical TiO_2 macropore–ZnO nanorod composite photoelectrode has been used in QDs based photoelectrochemical cells and showed excellent photocurrent density.[29] On the basis of our previous work about the successful fabrication of macroporous Zn_2SnO_4 photoelectrode and the superior properties of one-dimensional ZnO nanorod, it is highly

Received: August 23, 2013
Accepted: November 5, 2013
Published: November 5, 2013

desirable to integrate them together as a composite photoelectrode for solar cell application.

In this article, for the first time we report the fabrication of a novel macroporous Zn_2SnO_4–ZnO nanorod composite photoanode, and it was subsequently applied in CdS–CdSe QDs co-sensitized solar cells. The photovoltaic performance of the QDSSC based on macroporous Zn_2SnO_4–ZnO nanorod composite photoanode (1.68%) is much higher than that of pristine macroporous Zn_2SnO_4 photoanode (1.25%) with the same thickness (6 μm) which can be attributed to the enhanced surface area and superior light scattering ability resulting from the additional growth of ZnO nanorods. After optimization of the film thickness for such a composite photoanode, the best photovoltaic performance of 2.08% is achieved. To the best of our knowledge, this is the highest power conversion efficiency for the QDSSC related with Zn_2SnO_4 based photoelectrode.

EXPERIMENTAL SECTION

Preparation of the Macroporous Zn_2SnO_4 Film. Synthesis of the 750 nm PS spheres was performed in an emulsifier-free system.[38] Briefly, 73 g of styrene was added into 670 mL of distilled water at 70 °C under N_2 atmosphere, and after stirring for 15 min, 50 mL of 2.76 mM $K_2S_2O_8$ was dropped into the solution. Stirring was kept on for 24 h, and then the 750 nm PS spheres were obtained. Zn_2SnO_4 nanoparticle-covered PS spheres (Zn_2SnO_4@PS) were prepared through a hydrothermal process according to the previous report.[23] Briefly, 1.76 g of $Zn(CH_3COO)_2{\cdot}2H_2O$, 1.40 g of $SnCl_4{\cdot}5H_2O$, 16 mL of diethanolamine, and 16 mL of as-prepared PS spheres solution (0.087 g/mL) were dissolved in a mixed solvent of 16 mL of distilled water and 32 mL of 1,2-propylene glycol in a 100 mL Teflon-lined stainless steel autoclave. After vigorous stirring for 30 min, the autoclave was heated to 200 °C for 24 h. When the hydrothermal reaction finished, the resulted precipitates were rinsed with ethanol and distilled water and then dispersed in ethanol. The Zn_2SnO_4@PS ethanol solution (0.7 g/mL) was then dropped onto FTO glass (14 Ω/square, Nippon Sheet Glass, Japan) and dried naturally at room temperature. Films with different thicknesses were obtained by dropping different volumes of the solution. The films were then calcined at 500 °C for 1 h with a heating speed of 2 °C min^{-1} which formed an ordered macroporous Zn_2SnO_4 film.

Preparation of the Composite Zn_2SnO_4 Macropore–ZnO Nanorod Film. To prepare the ZnO sol, 0.6 M $Zn(CH_3COO)_2{\cdot}2H_2O$ was first added in 25 mL of ethanol at 50 °C. After stirring for 2 h, 1.5 mL of diethanolamine was added, and the mixture was stirred for another 2 h to obtain a clear ZnO sol solution. The above macroporous Zn_2SnO_4 film was spin-coated with the ZnO sol and then heated to 300 °C for 30 min. After cooling down to room temperature, the ZnO seeded macroporous Zn_2SnO_4 film was immersed into a 25 mM $Zn(NO_3)_2$ and hexamethylenetetramine (HMTA) aqueous solution in a Teflon autoclave (90 °C, 6 h) for the hydrothermal growth of ZnO nanorod.

Electrodeposition of CdS–CdSe QDs. The Zn_2SnO_4 or Zn_2SnO_4–ZnO film was used as the working electrode and a graphite rod was used as the counter electrode. For electrodeposition of CdS, the electrolyte contained 0.2 M $Cd(NO_3)_2$ and 0.2 M of thiourea in a 1/1 (v/v) dimethyl sulfoxide (DMSO)/water solution. The electrodeposition was proceeded with a constant current of 0.625 mA cm^{-2}, and it lasted for 20 min in a 90 °C water bath. For electrodeposition of CdSe, the electrolyte contained 0.02 M of $Cd(CH_3COO)_2$, 0.04 M of ethylene diamine tetraacetic acid disodium salt (EDTA), and 0.02 M of new prepared Na_2SeSO_3 which was obtained by refluxing 0.48 g of Se powder and 2.0 g of Na_2SO_3 in water at 100 °C for 3 h, and the solution had a pH of about 8.0–8.4. The electrodeposition was performed with a constant current of 0.625 mA cm^{-2} as well but it lasted for 30 min at room temperature.

Characterization of Zn_2SnO_4 or Zn_2SnO_4–ZnO Film. The film morphology and distribution of the elements were examined by field emission scanning electron microscopy and elemental mapping by energy dispersive spectroscopy (FE-SEM and EDS mapping, JSM-6330F). Transmission electron microscopy (TEM, JEOL-2010 HR) and X-ray diffractometry (XRD, Bruker D8 Advance) were also used for further structural and phase identification of the samples. UV/vis diffuse reflectance spectra were used to investigate light scattering ability of the films (without QDs), and absorption spectra was used to investigate the light harvesting property of the films with QDs loaded. Both these two measurements were performed on a UV/vis–NIR spectrophotometer (UV, Shimadzu UV-3150). The film thickness was measured by a profilometer (Ambios, XP-1).

Fabrication and Characterization of QDSSCs. The as-prepared Zn_2SnO_4 or Zn_2SnO_4–ZnO photoanodes were sandwiched together with Pt-counter electrodes. Polysulfide electrolyte was employed in our QDSSCs, and it contains 1 M sulfur powder, 1 M Na_2S, and 0.1 M NaOH dissolved in methanol/water (7:3, v/v). The active area of the QDSSCs is 0.16 cm^2. The current density–voltage (J–V) curves of the photoanodes were researched by applying a Keithley 2400 source meter under simulated AM 1.5 G illumination (100 mW cm^{-2}) provided by a solar simulator (91192, Oriel), and the light intensity was calibrated with a NREL-calibrated Si solar cell. The incident-photon-to-current efficiency (IPCE) spectra were analyzed in the wavelength range from 380 to 800 nm on the basis of a Spectral Products DK240 monochromator. The electrochemical impedance spectroscopy (EIS) measurement was carried out on the Zahner-Zennium electrochemical workstation in dark condition. The applied biases were equal to the negative value of V_{oc} for each sample, and the amplitude is 10 mV for the bias and the frequency ranged from 0.01 Hz to 1 MHz. Intensity-modulated photovoltage spectroscopy (IMVS) were also performed on the Zahner-Zennium electrochemical workstation. An intensity modulated (30–150 W m^{-2}) blue light emitting diode (457 nm) driven by a Zahner (PP211) source supply was used as the frequency response analyzer. The frequency ranged from to 0.1 Hz to 100 kHz. The modulated light intensity was 10% or less than the base light intensity.

RESULTS AND DISCUSSION

Hierarchical macroporous Zn_2SnO_4 film was prepared via a drop-casting process, and an aqueous solution containing Zn_2SnO_4 nanoparticles (4.2 nm in particle size) covered polystyrene (PS) spheres (750 nm in diameter) synthesized via an in situ hydrothermal method was dropped onto the conducting surface of the FTO glass, which then went through room temperature evaporation self-assembly that was followed by calcination to remove the PS spheres which lead to an ordered macroporous Zn_2SnO_4 film.[25] To prepare macroporous Zn_2SnO_4–ZnO nanorod composite film, ZnO seed layer was first covered on the macroporous Zn_2SnO_4 film via a spin-coating step, and then the film was immersed into zinc nitrate solution to perform a hydrothermal reaction which led to the growth of short ZnO nanorods and hence the formation of the interesting macroporous Zn_2SnO_4–ZnO nanorod composite film. Finally, the CdS and CdSe quantum dots were electrodeposited successively on the macroporous Zn_2SnO_4 or Zn_2SnO_4–ZnO based film for QDSSCs applications. The macroporous Zn_2SnO_4, Zn_2SnO_4–ZnO composites, and CdS/CdSe QDs co-sensitized photoanode are outlined in Scheme 1.

The morphology and structure of the macroporous Zn_2SnO_4 based film was further characterized by SEM and TEM. Figure 1a,b shows the top-view and cross-sectional field emission scanning electron microscopy (FE-SEM) images of a 6 μm thick macroporous Zn_2SnO_4 film on FTO glass. One can notice that the ordered Zn_2SnO_4 macroporous structure was formed and adhered onto the FTO glass via the present drop-casting process (Figure 1b). The average diameter of the Zn_2SnO_4 pores is about 650 nm (Figure 1a and the inset), which is

Scheme 1. Preparation Process of the QD-Sensitized Zn_2SnO_4–ZnO Composite Photoanode

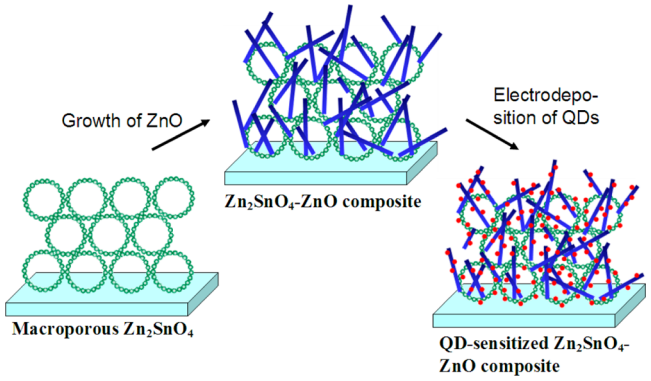

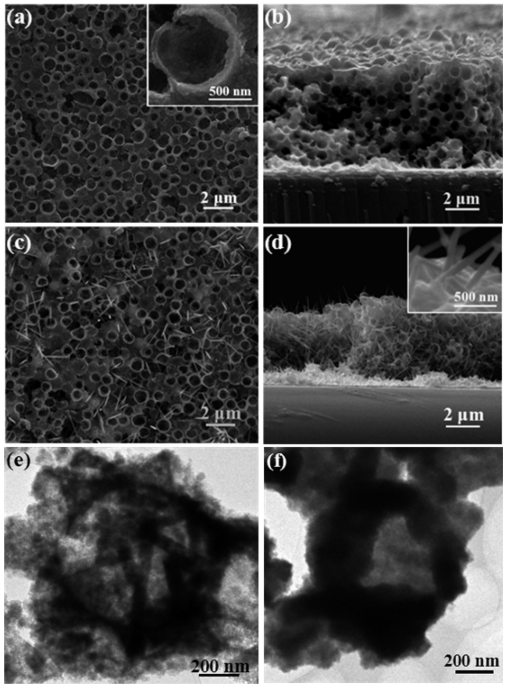

Figure 1. Top-view (a) and cross-sectional (b) FE-SEM images of the macroporous Zn_2SnO_4 film. Top-view (c), cross-sectional (d) FE-SEM and TEM images (e) of the composite Zn_2SnO_4–ZnO film. (f) TEM image of the composite film loaded with CdS–CdSe QDs.

slightly smaller than that of the original PS spheres (750 nm). After the subsequent hydrothermal reaction of Zn_2SnO_4 macroporous film in the zinc nitrate solution, many short ZnO nanorods can be observed from the top-view (Figure 1c) and cross-sectional FE-SEM images (Figure 1d). Specifically, ZnO nanorods with diameter of 80–120 nm and lengths ranged from several hundreds of nanometers to 2 μm were grown on the inside and surface of the Zn_2SnO_4 macroporous film. The transmission electron microscopy (TEM) image of Zn_2SnO_4–ZnO composite film (Figure 1e) illustrates that the macroporous Zn_2SnO_4 framework consists of nanoparticles and a few ZnO nanorods with diameter of about 80–120 nm grown on the margins of the pores. It is interesting to note that this is the first time the facile fabrication of Zn_2SnO_4 macropore–ZnO nanorod composite material has been reported. XRD spectra (Figure 2) reveal that the macroporous film can be indexed as Zn_2SnO_4 crystals (JCPDS Card No. 24-1470) with high purity and the composite film consists of Zn_2SnO_4 crystals

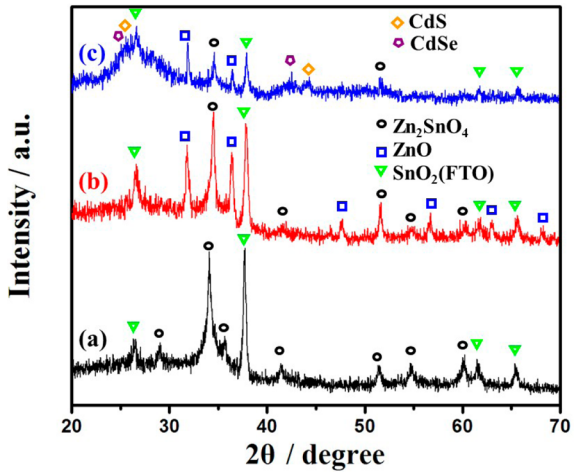

Figure 2. XRD patterns of the macroporous Zn_2SnO_4 (a), macroporous Zn_2SnO_4–ZnO nanorod (b), and electrodeposited CdS/CdSe co-sensitized macroporous Zn_2SnO_4–ZnO nanorod (c) film.

and ZnO crystals with hexagonal wurtzite structure (JCPDS Card No. 65-3411).

To explore their photoelectronic applications, the present macroporous Zn_2SnO_4 and the composite film with ZnO nanorods are used as photoelectrodes for quantum dot-sensitized solar cells. Electrodeposition is considered as a much more convenient and efficient method for the adsorption of QDs onto wide band-gap semiconductor materials compared to the CBD and SILAR method.[4,39] Herein, CdS and CdSe QDs are sequentially electrodeposited on the Zn_2SnO_4 macropore–ZnO nanorod composite film as referred to in our previous report.[4] According to the TEM images, after electrodeposition, both the macroporous Zn_2SnO_4 framework and the ZnO nanorods are well covered with CdS and CdSe QDs compactly (Figure 1f). The existence of cubic CdS (JCPDS Card No. 75-1546) and cubic CdSe (JCPDS Card No. 19-0191) can also be confirmed by the XRD spectra (Figure 2, curve c). Additionally, the FE-SEM images of the CdS/CdSe deposited Zn_2SnO_4 macropore–ZnO nanorod composite film (Figure 3a,b) show that both Zn_2SnO_4 and ZnO are hard to distinguish because of the compact coverage of QDs on them, which is significantly different from the undeposited film (Figure 1c,d). Further elemental mapping images measured by energy dispersive spectroscopy (Figure 3b, red square) confirm that the QDs elements such as Cd, S, and Se are distributed evenly across top to bottom of the cross-section of the Zn_2SnO_4 macropore–ZnO nanorod composite film (Figure 3c).

Figure 4a shows the photocurrent density–photovoltage (J–V) curves of QDSSCs based on the 6 μm thick pristine macroporous Zn_2SnO_4 photoanode and the Zn_2SnO_4 macropore–ZnO nanorod composite photoanode, and the detailed photovoltaic parameters are listed in Table 1. The short-circuit current density (J_{sc}), open-circuit voltage (V_{oc}), fill factor (FF), and power conversion efficiency (η) are 7.11 mA cm^{-2}, 519 mV, 0.34, and 1.25% for the pristine Zn_2SnO_4 photoanode. Compared with the previously reported Zn_2SnO_4 nanowires based CdSe QDSSC (0.3%),[26] here, the η has been significantly promoted due to the utilization of macroporous structure and CdS/CdSe co-sensitization. For the Zn_2SnO_4 macropore–ZnO nanorod composite photoanode, the corresponding parameters

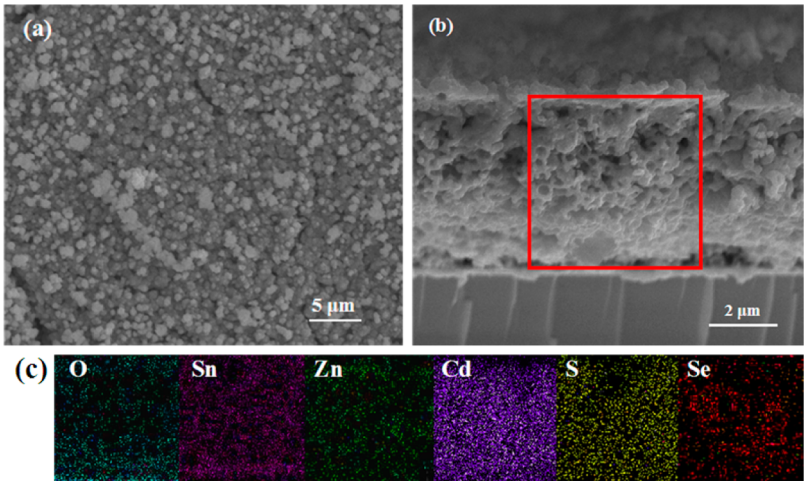

Figure 3. Top-view (a) and (b) cross-sectional FE-SEM images of the composite Zn_2SnO_4–ZnO film after electrodeposition of CdS–CdSe QDs. Image (c) is elemental mapping by energy dispersive spectroscopy for the rectangular area indicated by a red square in (b).

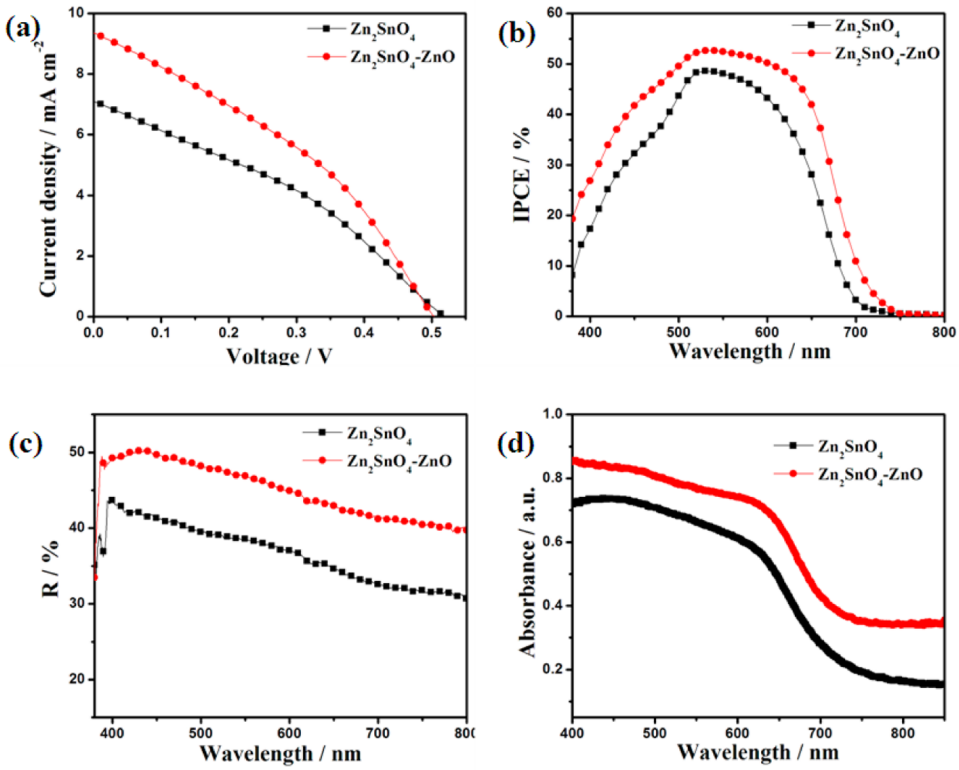

Figure 4. (a) *J*–*V* curves and (b) IPCE curves of QDSSCs fabricated with Zn_2SnO_4 and Zn_2SnO_4–ZnO photoanodes. UV–vis diffused reflectance spectra (c) and absorption spectra (d) of the pristine Zn_2SnO_4 and Zn_2SnO_4–ZnO composite films before and after electrodeposition of CdS/CdSe QDs.

are 9.36 mA cm^{-2}, 503 mV, 0.36, and 1.68%, respectively. The impressive enhancement of J_{sc} (from 7.11 to 9.36 mA cm^{-2}) can be ascribed to higher surface area and excellent light scattering property of the Zn_2SnO_4–ZnO composite film compared to the pristine Zn_2SnO_4 macroporous film, which results in higher light-harvesting efficiency and thus leads to high power conversion efficiency. It is well known that the incident-photon-to-current efficiency (IPCE) was dominated by light-harvesting efficiency, quantum yield of electron injection, and efficiency of collecting the injected electrons, and the IPCE spectra based on the pristine Zn_2SnO_4 and Zn_2SnO_4–ZnO composite films are shown in Figure 4b. Evidently, the IPCE value of the composite photoanode based QDSSCs is larger than that of pristine Zn_2SnO_4 photoanode based QDSSCs in the measured wavelength range from 380 nm to 750 nm, and it also displays a red-shift to a longer wavelength of about 650–750 nm. These results indicate that the composite photoanode has better light harvesting and scattering ability than the pristine one which correlates well with the aforementioned higher J_{sc}. Moreover, FE-SEM images (Figure 1e) show the fact that many ZnO nanorods grow between the interspaces of the Zn_2SnO_4 pores in the composite film, and such a composite structure can not only enlarge the surface area but also facilitate the light scattering property.

Table 1. Detailed Photovoltaic Parameters of QDSSCs Based on the Zn_2SnO_4 Photoanode with 6 μm Thick Film and Zn_2SnO_4–ZnO Photoanodes with Different Film Thicknesses

photoanode	J_{sc}, mA·cm^{-2}	V_{oc}, mV	FF	η, %
6 μm Zn_2SnO_4	7.11	519	0.34	1.25
6 μm Zn_2SnO_4–ZnO	9.36	503	0.36	1.68
9 μm Zn_2SnO_4–ZnO	11.32	492	0.37	2.08
13 μm Zn_2SnO_4–ZnO	9.95	479	0.36	1.73
16 μm Zn_2SnO_4–ZnO	7.95	467	0.38	1.42
20 μm Zn_2SnO_4–ZnO	7.04	394	0.38	1.05

Figure 4c is the UV–vis diffused reflectance spectra of the pristine Zn_2SnO_4 and Zn_2SnO_4–ZnO composite films, which reveals that the reflectance of the latter is higher than that of the former in the wavelength range from 400 to 800 nm, implying better light scattering ability for the Zn_2SnO_4–ZnO composite film. After the electrodeposition of CdS and CdSe QDs, the Zn_2SnO_4–ZnO composite film shows obvious higher absorption values throughout the visible region from the absorption spectra (Figure 4d), indicating better light harvesting efficiency for this combined structured photoanode. Consequently, the enlargement of the surface area due to additional growth of ZnO nanorods in the macroporous Zn_2SnO_4 framework for a larger amount of QD loading and improved light scattering ability can greatly contribute to remarkable enhancement of J_{sc} for the composite photoanode. Though the Zn_2SnO_4–ZnO composite photoanode (503 mV) shows a slightly lower V_{oc} compared to the pristine Zn_2SnO_4 based photoanode (519 mV), the power conversion efficiency for the former (1.68%) has witnessed a 34.4% enhancement compared to the latter one (1.25%), which is mainly ascribed from the much higher J_{sc}.

Electrochemical impedance spectroscopy (EIS) measurement was employed to study the interfacial charge transfer process within QDSSCs based on Zn_2SnO_4 photoanode or Zn_2SnO_4–ZnO composite photoanode. Figure 5a is the Nyquist plots of QDSSCs based on these two photoanodes, which shows one defined semicircle in the low frequency region, and this dominates the spectra for both of the two photoanodes.[18] The semicircle in the low frequency corresponds to the electron transfer at the Zn_2SnO_4(–ZnO)/QDs/electrolyte interface. Clearly, the recombination resistance of pristine macroporous Zn_2SnO_4 photoanode was larger than the Zn_2SnO_4–ZnO composite one, indicating slower electron recombination rate within QDSSCs for the former.[40,41] Slower charge recombination is commonly related to higher V_{oc} for the pristine Zn_2SnO_4 based solar cell, which is consistent with the J–V measurement. The decrease of V_{oc} for the Zn_2SnO_4–ZnO composite photoanode can be ascribed to the enlargement of its surface area, which probably brings about more trapping sites for electron recombination.

To further investigate the dynamics of charge recombination in the solar cells, intensity-modulated photovoltage spectroscopy (IMVS) was applied for the characterization. The electron life time τ_n can be calculated by the equation $\tau_n = 1/(2\pi f_{IMVS})$, where f_{IMVS} is the characteristic minimum frequency of the IMVS imaginary component.[42] The calculated τ_n result as a function of light intensities is shown in Figure 5b. The longer electron lifetime for the QDSSCs based on the pristine Zn_2SnO_4 photoanode indicates slower charge recombination which is consistent with the EIS result. In the composite film, ZnO nanorods grew on the margins of the pores and protrude into the spaces of the pores, which led to more trapping sites for electron recombination. However, the enlargement of surface area anchoring the larger amount of deposited QDs and the superior light scattering capability greatly contribute to the enhanced J_{sc}, which compensates for the inferior V_{oc} behavior and thus leads to promising power conversion efficiency.

To investigate the effects of film thickness on the photovoltaic performance of CdS/CdSe QDSSCs and further improve the power conversion efficiency, Zn_2SnO_4 macropore–ZnO nanorod composite films with five different thicknesses (6, 9, 13, 16, 20 μm) were prepared. Figure 6 displays the J–V curves of QDSSCs based on Zn_2SnO_4–ZnO composite photoelectrodes with different thicknesses, and Table 1 summarizes the detailed photovoltaic parameters. When the film thickness rises from 6 μm to 9 μm, J_{sc} enhances significantly from 9.36 to 11.32 mA cm^{-2}. In spite of the slight decrease of V_{oc}, the 9 μm thick composite film exhibits an impressive power conversion efficiency of 2.08%. However, with continuously increasing the film thickness to 13, 16, and 20 μm, both J_{sc} and V_{oc} decrease and thus efficiencies of the QDSSCs drop to 1.73, 1.42, and 1.05%, respectively. The thicker the film is, the more trapping sites and recombination centers for the electrons, which leads to the decrease of V_{oc} for thicker films. For the J_{sc}, when increasing film thickness from 6 μm to 9 μm, the thicker film is able to adsorb much more CdS/CdSe QDs, which enhances the light harvesting ability of the photoanode and the quantity of photogenerated electrons.

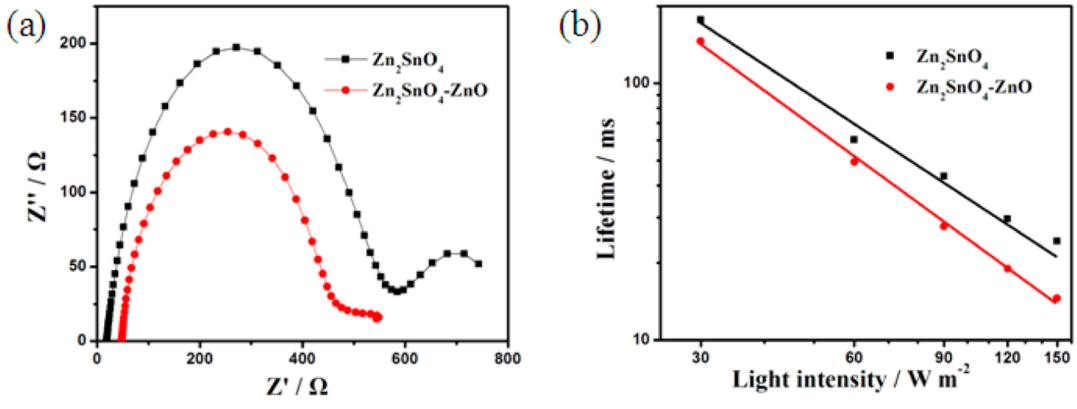

Figure 5. EIS spectra (a) and lifetime constants (b) measured by the IMVS test of the QDSSCs based on the electrodeposited CdS/CdSe co-sensitized Zn_2SnO_4 and Zn_2SnO_4–ZnO photoanodes.

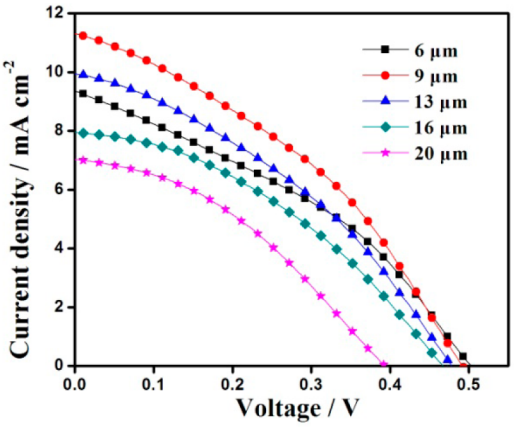

Figure 6. Comparison of $J-V$ curves for QDSSCs fabricated with composite photoanodes with different film thicknesses.

When the film increases to 13 μm or thicker, the serious electron recombination in the thick films reduces the concentration of electrons, which counteracts the contribution of the higher QD loading and hence leads to the obvious decline of J_{sc} for the QDSSCs using photoanode films with thickness over 9 μm.

CONCLUSION

In summary, a macroporous Zn_2SnO_4–ZnO nanorod composite photoelectrode was prepared via a drop-casting and subsequent hydrothermal process for the first time, and such novel hierarchical micro-/nano-structured photoelectrode was further used as photoanode for the QDSSC application. QDSSCs based on the electrodeposited CdS and CdSe QDs co-sensitized Zn_2SnO_4 macropore–ZnO nanorod composite film shows an impressive photovoltaic performance (1.68%) which has a 34.4% enhancement compared to the pristine macroporous Zn_2SnO_4 (1.25%) for the constant thickness of 6 μm. UV–vis absorption, diffused spectra, and IPCE spectra reveal that the growth of ZnO nanorods mostly contributes to the enlargement of surface area and improvement of light scattering ability of the composite film, which dominates the increase of J_{sc} values and eventual power conversion efficiency. EIS and IMVS results show that the additional ZnO nanorods in the composite photoelectrode would provide additional trapping sites for electron recombinations within QDSSCs and thus lead to a slightly lower V_{oc} compared to the pristine macroporous Zn_2SnO_4. Further optimization of the Zn_2SnO_4 macropore–ZnO nanorod composite film thickness and the power conversion efficiency of 2.08% were attained with a thickness of 9 μm, which is the highest value for the reported QDs sensitized solar cells based on the Zn_2SnO_4 photoelectrode. Further enhancement of photovoltaic performance can be expected by growing a larger amount of ZnO nanorods, loading wide spectrum absorption QDs (CdTe, perovskite), and using other counter electrodes (Cu_2S etc.).

AUTHOR INFORMATION

Corresponding Author

*E-mail: kuangdb@mail.sysu.edu.cn.

Notes

The authors declare no competing financial interest.

ACKNOWLEDGMENTS

The authors acknowledge the financial support from the National Natural Science Foundation of China (91222201, U0934003), the Program for New Century Excellent Talents in University (NCET-11-0533), the Fundamental Research Funds for the Central Universities, the Research Fund for the Doctoral Program of Higher Education (20100171110014), and the NSF of Guangdong Province (S2013030013474).

REFERENCES

(1) Grätzel, M. *Nature* **2001**, *414*, 338–344.
(2) Kamat, P. V.; Tvrdy, K.; Baker, D. R.; Radich, J. G. *Chem. Rev.* **2010**, *110*, 6664–6688.
(3) Nozik, A. J.; Beard, M. C.; Luther, J. M.; Law, M.; Ellingson, R. J.; Johnson, J. C. *Chem. Rev.* **2010**, *110*, 6873–6890.
(4) Yu, X. Y.; Liao, J. Y.; Qiu, K. Q.; Kuang, D. B.; Su, C. Y. *ACS Nano* **2011**, *5*, 9494–9500.
(5) Shengyuan, Y.; Nair, A. S.; Josec, R.; Ramakrishna, S. *Energy Environ. Sci.* **2010**, *3*, 2010–2014.
(6) Sun, W. T.; Yu, Y.; Pan, H. Y.; Gao, X. F.; Chen, Q.; Peng, L. M. *J. Am. Chem. Soc.* **2008**, *130*, 1124–1125.
(7) Han, H.; Sudhagar, P.; Song, T.; Jeon, Y.; Mora-Seró, I.; Fabregat-Santiago, F.; Bisquert, J.; Kang, Y. S.; Paik, U. *Chem. Commun.* **2013**, *49*, 2810–2812.
(8) Wang, H.; Miyauchi, M.; Ishikawa, Y.; Pyatenko, A.; Koshizaki, N.; Li, Y.; Li, L.; Li, X.; Bando, Y.; Golberg, D. *J. Am. Chem. Soc.* **2011**, *133*, 19102–19109.
(9) Zhu, Z.; Qiu, J.; Yan, K.; Yang, S. *ACS Appl. Mater. Interfaces* **2013**, *5*, 4000–4005.
(10) Sun, B.; Hao, Y.; Guo, F.; Cao, Y.; Zhang, Y.; Li, Y.; Xu, D. *J. Phys. Chem. C* **2012**, *116*, 1395–1400.
(11) Kim, H.; Yong, K. *Phys. Chem. Chem. Phys.* **2013**, *15*, 2109–2116.
(12) Coutts, T. J.; Young, D. L.; Li, X.; Mulligan, W. P.; Wu, X. *J. Vac. Sci. Technol. A* **2000**, *18*, 2646–2660.
(13) Breckenridge, R. G.; Hoslter, W. R. *Phys. Rev.* **1953**, *91*, 793–802.
(14) Villarreal, T. L.; Boschloo, G.; Hagfeldt, A. *J. Phys. Chem. C* **2007**, *111*, 5549–5556.
(15) Tan, B.; Toman, E.; Li, Y.; Wu, Y. *J. Am. Chem. Soc.* **2007**, *129*, 4162–4163.
(16) Kim, D. W.; Shin, S. S.; Cho, I. S.; Lee, S.; Kim, D. H.; Lee, C. W.; Jung, H. S.; Hong, K. S. *Nanoscale* **2012**, *4*, 557–562.
(17) Chen, J.; Lu, L.; Wang, W. *J. Phys. Chem. C* **2012**, *116*, 10841–10847.
(18) Li, Z.; Zhou, Y.; Bao, C.; Xue, G.; Zhang, J.; Liu, J.; Yu, T.; Zou, Z. *Nanoscale* **2012**, *4*, 3490–3494.
(19) Choi, S. H.; Hwang, D.; Kim, D. Y.; Kervella, Y.; Maldivi, P.; Jang, S. Y.; Demadrille, R.; Kim, I. D. *Adv. Funct. Mater.* **2013**, *23*, 3146–3155.
(20) Miyauchi, M.; Liu, Z.; Zhao, Z. G.; Anandan, S.; Hara, K. *Chem. Commun.* **2010**, *46*, 1529–1531.
(21) Huang, L.; Jiang, L.; Wei, M. *Electrochem. Commun.* **2010**, *12*, 319–322.
(22) Li, Y.; Wang, Y.; Chen, C.; Pang, A.; Wei, M. *Chem.—Eur. J.* **2012**, *18*, 11716–11722.
(23) Wang, Y. F.; Li, K. N.; Xu, Y. F.; Rao, H. S.; Su, C. Y.; Kuang, D. B. *Nanoscale* **2013**, *5*, 5940–5948.
(24) Li, Y.; Pang, A.; Zheng, X.; Wei, M. *Electrochim. Acta* **2011**, *56*, 4902–4906.
(25) Li, Y.; Guo, B.; Zheng, X.; Pang, A.; Wei, M. *Electrochim. Acta* **2012**, *60*, 66–70.
(26) Dai, Q.; Chen, J.; Lu, L.; Tang, J.; Wang, W. *Nano Lett.* **2012**, *12*, 4187–4193.
(27) Bora, T.; Kyaw, H. H.; Dutta, J. *Electrochim. Acta* **2012**, *68*, 141–145.
(28) Bai, Y.; Yu, H.; Li, Z.; Amal, R.; G. Lu, Q. M.; Wang, L. *Adv. Mater.* **2012**, *24*, 5850–5856.

(29) Karuturi, S. K.; Luo, J.; Cheng, C.; Liu, L.; Su, L. T.; Tok, A. I. Y.; Fan, H. J. *Adv. Mater.* **2012**, *24*, 4157−4162.
(30) Tian, J.; Zhang, Q.; Zhang, L.; Gao, R.; Shen, L.; Zhang, S.; Qu, X.; Cao, G. *Nanoscale* **2013**, *5*, 936−943.
(31) Yin, Z.; Wang, Z.; Du, Y.; Qi, X.; Huang, Y.; Xue, C.; Zhang, H. *Adv. Mater.* **2012**, *24*, 5374−5378.
(32) Qian, J.; Liu, P.; Xiao, Y.; Jiang, Y.; Cao, Y.; Ai, X.; Yang, H. *Adv. Mater.* **2009**, *21*, 3663−3667.
(33) Liu, M.; Yang, J.; Feng, S.; Zhu, H.; Zhang, J.; Li, G.; Peng, J. *Mater. Lett.* **2012**, *76*, 215−218.
(34) Yang, S. C.; Yang, D. J.; Kim, J.; Hong, J. M.; Kim, H. G.; Kim, I. D.; Lee, H. *Adv. Mater.* **2008**, *20*, 1059−1064.
(35) Tétreault, N.; Arsenault, É.; Heiniger, L. P.; Soheilnia, N.; Brillet, J.; Moehl, T.; Zakeeruddin, S.; Ozin, G. A.; Grätzel, M. *Nano Lett.* **2011**, *11*, 4579−4584.
(36) Mandlmeier, B.; Szeifert, J. M.; Fattakhova-Rohlfing, D.; Amenitsch, H.; Bein, T. *J. Am. Chem. Soc.* **2011**, *133*, 17274−17282.
(37) Li, K. N.; Wang, Y. F.; Xu, Y. F.; Chen, H. Y.; Su, C. Y.; Kuang, D. B. *ACS Appl. Mater. Interfaces* **2013**, *5*, 5105−5111.
(38) Goodwin, J. W.; Hearn, J.; Ho, C. C.; Ottewill, R. H. *Colloid Polym. Sci.* **1974**, *252*, 464−471.
(39) Wang, X.; Zhu, H.; Xu, Y.; Wang, H.; Tao, Y.; Hark, S.; Xiao, X.; Li, Q. *ACS Nano* **2010**, *4*, 3302−3308.
(40) Lagemaat, J.; Park, N. G.; Frank, A. J. *J. Phys. Chem. B* **2000**, *104*, 2044−2052.
(41) Wang, Q.; Ito, S.; Grätzel, M.; Fabregat-Santiago, F.; Mora-Seró, I.; Bisquert, J.; Bessho, T.; Imai, H. *J. Phys. Chem. B* **2006**, *110*, 25210−25221.
(42) Schlichthorl, G.; Huang, S. Y.; Sprague, J.; Frank, A. J. *J. Phys. Chem. B* **1997**, *101*, 8141−8155.